

# TiC Lattice Dynamics from *ab initio* Calculations

P.T. Jochym, K. Parlinski, and M. Sternik

Institute of Nuclear Physics, ul. Radzikowskiego 152, 31-342 Cracow, Poland

the date of receipt and acceptance should be inserted later

**Abstract.** *Ab initio* calculations and a direct method have been applied to derive the phonon dispersion curves and phonon density of states for the TiC crystal. The results are compared and found to be in a good agreement with the experimental neutron scattering data. The force constants have been determined from the Hellmann-Feynman forces induced by atomic displacements in the  $2 \times 2 \times 2$  supercell. The calculated phonon density of states suggests that vibrations of Ti atoms form acoustic branches, whereas the motion of C atoms is confined to optic branches. The elastic constants have been found using the deformation method and compared with the results obtained from acoustic phonon slopes.

**PACS.** 63.20.-e Phonons and vibrations in crystal lattices – 71.15.N Total energy calculations

The transition-metal carbide compounds, of which TiC is a representative, are of big scientific and technological interest because of their striking mechanical properties, extreme hardness combined additionally with metallic electrical and thermal conductivity. They have usually a rock-salt crystal structure – like some ionic crystals – while having properties typical for materials with covalent bonding. It suggests that the bonding have some mixed nature, which makes these materials very interesting as an object of study.

Over a large range of fractional carbon content from TiC to  $\text{TiC}_{0.5}$  [1] the TiC is stable in the NaCl structure, with space group  $\text{Fm}\bar{3}\text{m}$ . In practice, it is usually non-stoichiometric and contains carbon vacancy defects. The phonon dispersion curves of nearly stoichiometric  $\text{TiC}_{0.95}$  have been measured along main symmetry directions by Pintschovius et al [2] using the inelastic neutron scattering technique. In the same paper, the influence of the carbon content on the phonon dispersion curves has been additionally checked by measuring a sample with lower carbon concentration  $\text{TiC}_{0.89}$ . The results shown that the optic modes could differ by 3.5%, while the acoustic modes are less sensitive to carbon content. The elastic constants derived from the measured acoustic dispersion curves agree very well with those obtained by ultrasonic measurements for  $\text{TiC}_{0.91}$  crystal [3].

Very interesting properties and simple structure of TiC caused that efforts to understand its properties using first-principle calculations have been undertaken several times [4, 5, 6, 7]. The electronic structure, bulk modulus, and elastic constants have been found [8] by means of accurate first-principles total-energy calculations using the full potential linear muffin-tin orbital method. The calculated

values are generally in very good agreement with experiment.

In this paper we intend to extend first-principle calculations to describe the phonon dispersion curves and phonon density of TiC. The method which was based on the total energy calculation and *Hellmann-Feynman* (HF) forces. Dispersion relations are calculated by *direct method* [9, 10, 11, 12, 13], in which the force constants of the dynamical matrix are calculated from HF forces. Elastic constants and bulk modulus have been estimated by straight evaluation of energy derivatives with respect to deformation.

The energies and forces of the TiC crystal were calculated by the method of total energy minimization, using a norm-conserving *pseudopotentials* as an approximation of the atomic core – valence electron interaction [14, 15]. For an excellent review of *ab initio* total-energy calculations see Ref.[16] and further references given there. For the lattice dynamics calculations the  $2 \times 2 \times 2$  supercell with periodic boundary conditions and 64 atoms has been used. For optimizing the structure and for direct calculation of energy deformations  $1 \times 1 \times 1$  supercell has been utilized. The *ab initio* total energy calculations were done with the CASTEP package [17] and standard pseudopotentials provided within this package. These pseudopotentials were constructed within LDA approximation. The Ti pseudopotential treats 3p electrons as belonging to the core. We have employed non-local variant of those potentials parametrized in the reciprocal space with 900 eV and 600 eV cut-off energy for  $1 \times 1 \times 1$  and  $2 \times 2 \times 2$  supercell, respectively. Tests which had been made with the cut-off energy of 600 eV applied to the  $1 \times 1 \times 1$  supercell, showed that in this case the cohesive energy is only 0.2 eV higher, and the lattice constant is longer by  $0.0006 \text{ \AA}$  (0.01%), com-

paring to the 900 eV cut-off. Therefore, we have used 600 eV cut-off energy for a larger supercell calculation.

A *generalized gradient approximation* (GGA) has been used for the exchange energy term of the valence states of the Hamiltonian [18]. Although this procedure is not quite consistent, there are indications [19] that LDA generated pseudopotentials used with GGA exchange term in crystals are sufficiently accurate for energies and structures. The integration over the Brillouin zone has been performed with weighted summation over wave vectors generated by Monkhorst-Pack scheme [20] using  $0.1 \text{ \AA}^{-1}$  and  $0.06 \text{ \AA}^{-1}$  grid sizes which leads to 4 and 32 wave vectors for  $1 \times 1 \times 1$  supercell and to 1 and 4 wave vectors for  $2 \times 2 \times 2$  supercell, respectively. No significant difference due to different number of wave vectors, 1 or 4, has been found in calculated phonon frequencies. The results of dispersion curve presented here are generated from the  $0.06 \text{ \AA}^{-1}$  data set with 4 wave vectors.

Since TiC is a weakly metallic compound it could have been appropriate to use a smearing of electron levels in the Brillouin zone integration. This procedure is computationally more expensive. Thus we have performed a series of tests to compare lattice constants, bulk moduli and phonons in  $\Gamma$  and X points obtained using gaussian smearing in the range from 4 to 0.1 eV and denser k-space grids (4, 14, 32, 63 k-points) for one unit cell configuration. The comparison of results shown in the Table 1 indicate that, for sufficiently dense k-space grid used, these quantities are not very sensitive (specially the lattice constant and bulk modulus) to the choice of method of Brillouin zone integration. Thus we have decided to use much simpler and faster non-metallic approach in the final  $2 \times 2 \times 2$  supercell calculation. Note also that results obtained in the metallic regime lead to larger divergency of phonon frequencies from experimental data.

The minimization of the total energy with respect to the lattice constant was performed within the CASTEP minimizer module with  $1 \times 1 \times 1$  supercell and cross-checked with  $2 \times 2 \times 2$  supercell. The equilibrium lattice constant is  $a = 4.3448 \text{ \AA}$  which could be compared with the experimental value  $a = 4.3269 \text{ \AA}$  [21]. Such a good agreement may be coincidental, since inclusion of 3p electrons in the valence band as well as gradient corrections in core states tends to change the equilibrium lattice constant [22, 23, 24].

The HF forces are defined as

$$\mathbf{F}_i(\mathbf{n}, \nu) = -\partial E_{tot} / \partial \mathbf{R}_i(\mathbf{n}, \nu) \quad (1)$$

where  $\mathbf{n}, \nu$  are the indices of the unit cell and atom within the unit cell, respectively, and  $i$  is the Cartesian component. At extremum all HF forces vanish. Non-zero HF forces arise, when a single atom  $(\mathbf{m}, \mu)$  is displaced by  $u_j(\mathbf{m}, \mu)$  from its equilibrium position. The arising forces are related with the cummulant force constants  $\Phi_{ij}$  by a relation [11, 12]

$$\mathbf{F}_i(\mathbf{n}, \nu) = - \sum_{\mathbf{m}, \mu, j} \Phi_{ij}(\mathbf{n}, \nu; \mathbf{m}, \mu) u_j(\mathbf{m}, \mu) \quad (2)$$

Cummulant force constants appear as a result of periodic boundary conditions imposed on the supercell. To calculate HF forces an atomic configuration with a single displaced atom must be minimized with respect to the electronic part only. Each of such runs provides  $3n$  HF forces, where  $n = 8$  or  $64$  is the number of atoms in the  $1 \times 1 \times 1$  or  $2 \times 2 \times 2$  supercell, respectively. Two runs with displacements along  $z$  direction, one for Ti and second for C were performed. To minimize the systematic errors two other runs with negative displacements were carried on. The displacement amplitudes were set to 1% of the lattice constant. This amplitude has been selected after number of careful tests in which displacements were varied from 0.1% to 1.6%. It has been proven that the anharmonic contributions are negligible up to 1% of displacement. At smaller displacements, close to 0.1% the HF forces became too small and the uncertainty of force constant evaluation is not acceptable.

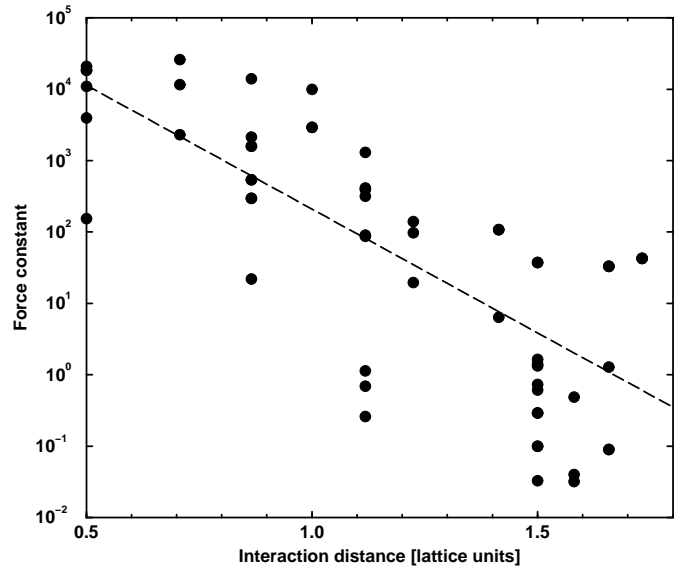


**Fig. 1.** Absolute eigenvalues of the force constant matrices of the TiC crystal as a function of interatomic distance.

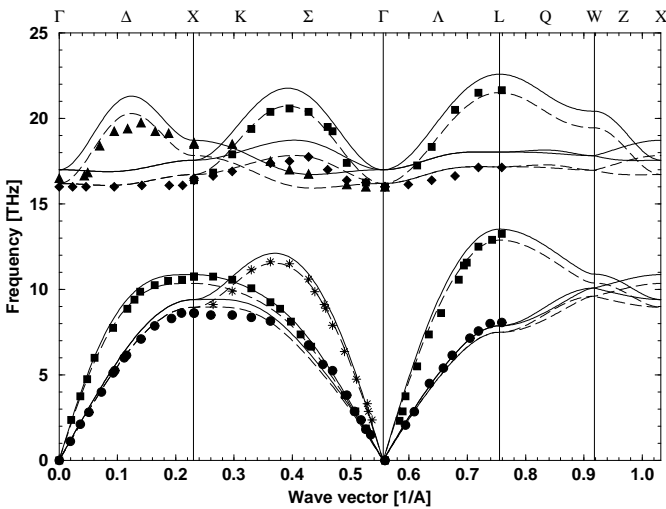
The data of  $4 \times 3n$  HF forces  $\mathbf{F}_i(\mathbf{n}, \nu)$  and four displacements  $u_j(\mathbf{m}, \mu)$  form an overdetermined set of equations, Eq.(2), for the force constants. This system was solved by the singular value decomposition algorithm [11, 25], which automatically provides the least-squares solution. For  $2 \times 2 \times 2$  supercell the 768 components of the HF forces lead to 33 non-zero independent parameters of the force constants. Knowledge of these force constants allows one to test the range of interaction potential. For that, similarly to procedure used in [13], we have calculated the absolute values of the eigenvalues of the  $3 \times 3$   $\Phi_{ij}(\mathbf{n}, \nu; \mathbf{m}, \mu)$  matrices and plotted them against a distance between atoms  $(\mathbf{n}, \nu)$  and  $(\mathbf{m}, \mu)$ . The result for  $2 \times 2 \times 2$  supercell is depicted in Fig. 1. It shows that the interaction drops down at least by two orders of magnitudes within the size of the supercell. The scatter of points is too large to assign any rule which could govern the decaying of

Quantity	Exper.	Non-metallic	Metallic			
# k		4	4	14	32	63
$a_0$	4.327	4.345	4.35	4.342	4.345	4.342
$B$	2.4	2.42	2.41	3.527	2.418	2.427
$\omega_\Gamma$	16.3	16.5	19.0	11.8	15.6	15.6
$\omega_X^1$	8.5	8.5	10.2	5.1	9.2	8.5
$\omega_X^2$	10.8	10.0	11.1	10.3	10.7	10.7
$\omega_X^3$	16.5	17.0	18.2	12.8	15.7	15.3
$\omega_X^4$	18.5	17.8	19.3	16.7	18.1	17.7

**Table 1.** Comparison of results from metallic and non-metallic approach

the force constants parameters with distance. From Fig. 1 it is clear that the  $1 \times 1 \times 1$  supercell is too small to be used for calculation of dispersion curves since the considered force constants terminate at radius of  $a\sqrt{3}/2 = 0.866a$ .

The knowledge of the cummulant force constants allows one to define an approximate dynamical matrix, in which the summation over all atoms is confined to those atoms which reside within the volume of the supercell. The approximate dynamical matrix becomes equal to the conventional one at discrete wave vectors  $\mathbf{k}_L$  given by the equation  $\exp(2\pi i \mathbf{k}_L \cdot \mathbf{L}) = 1$  [11], where  $\mathbf{L} = (\mathbf{L}_1, \mathbf{L}_2, \mathbf{L}_3)$  are the lattice vectors of the supercell. At the wave vectors  $\mathbf{k}_L$  the phonon frequencies  $\omega^2(\mathbf{k}_L)$ , calculated by diagonalization of the approximate dynamical matrix, are the same as those calculated from the exact dynamical matrix. For  $2 \times 2 \times 2$  supercell the exact wave vectors are at  $\Gamma$ , X, L, W, and two other wave vector points, namely, the midpoint between  $\Gamma$  and X along  $\langle 1, 0, 0 \rangle$  and  $\langle 1, 1, 1 \rangle$  directions. The advantage of the above described direct method is that it does not impose any limit to the range of interaction. When the supercell size is smaller than the range of interaction, the direct method interpolates the dispersion curves between the exact points.

**Fig. 2.** Phonon dispersion relations of TiC crystal calculated from  $2 \times 2 \times 2$  supercell (full line). The same dispersion curves divided by a factor 1.05 (dashed line). Experimental points taken from Ref. [2].

The dispersion curves calculated on the basis of  $2 \times 2 \times 2$  supercell are shown in Fig. 2. They correspond to temperature  $T=0$ . At the same Figure 2 we compare the calculated dispersion curves with the experimental phonon frequencies measured by the inelastic neutron scattering [2]. Different symbols of experimental points correspond to different phonon polarizations established experimentally.

The experimental points are about  $\Delta\omega = 0.05\omega$  lower than the calculated values. One of the reasons for such situation could be that experimental values are measured at room temperature and anharmonic effects might diminish the phonon frequencies. Another reason may be related with a non-stoichiometric concentration of carbon in measured samples, which diminish in average phonon frequencies as well. The effect that experimental phonon points are at lower frequencies than the calculated ones appears as well in other ab-initio calculations [9, 11].

The theory of lattice dynamics provides summation rules which follow from translational and rotational invariances of the crystal. For TiC these invariances lead to two equations, which can be used to set the values of on-site force constant parameters. If these conditions are satisfied the acoustic phonon branches at  $\mathbf{k}=0$  would point to  $\omega = 0$ . Our dispersion curves, without imposed translational-rotational invariances point at  $\mathbf{k}=0$  to  $\omega = 0.31\text{THz}$ . Since the invariance conditions should be satisfied within the *ab initio* and direct methods, we have not corrected our dispersion curves displayed in Fig. 2 according to this effect.

By sampling the dynamical matrix for many wave vectors, one can calculate the phonon density function  $g(\omega)$ , and the partial phonon density functions  $g_{x,Ti}(\omega)$  and  $g_{x,C}(\omega)$ . The  $g(\omega)$  describes the number of phonon frequencies in an interval around  $\omega$ , while  $g_{x,Ti}$  and  $g_{x,C}$  specify the number of phonon frequencies in the interval around  $\omega$  but modified by the population of the  $x$  displacement component of either Ti or C atom. The density of states functions are shown in Fig. 3. They are conventionally normalized to  $\int g(\omega)d\omega = 1$  and  $\int g_{x,\alpha}(\omega)d\omega = 1/6$ , where  $\alpha = \text{Ti or C}$ . The curves show that motions within acoustic dispersion curves are almost entirely due to Ti atoms. The sum of Titanium density functions ( $g_{x,Ti}(\omega) + g_{y,Ti}(\omega) + g_{z,Ti}(\omega)$ ) fits to the total density function  $g(\omega)$  below 14 THz. Part of  $g(\omega)$  above the gap is mainly due to C atoms. Thus, TiC form a rather special crystal, in which the Ti atoms, as heavier, form a frame for elastic motion, and the C atoms vibrate within the optical

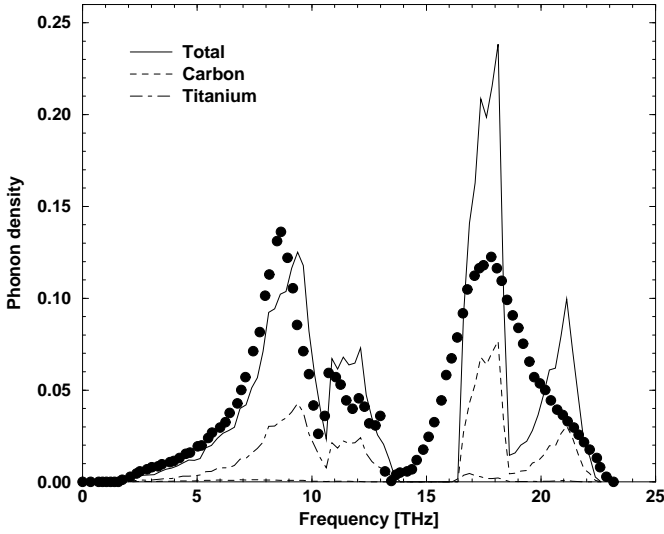


**Fig. 3.** Phonon density spectrum  $g(\omega)$  of the TiC crystal and partial phonon density spectra  $g_{i,\alpha}(\omega)$ , where  $\alpha = \text{C or Ti}$  and  $i = x, y$  or  $z$  are the displacement directions. Experimental points taken from Ref. [2].

modes. We add, however, that the magnitude of the force constants between Ti - C and between Ti - Ti and C - C at the same distances remains of the same order. Thus, TiC does not consist of two weakly bounded subsystems. In Fig. 3 the experimentally determined phonon density of states [2,26] is also shown. The agreement within acoustic region is quite good. In optic part the experimental resolution of  $\approx 2.5\text{THz}$  and the nonstoichiometry of carbon in the sample lead to broadening of the optic band.

The elastic constants can be evaluated from the slopes of acoustic branches of phonon dispersion curves. Here, we have used the invariance conditions to set the acoustic modes to  $\omega = 0$  at  $\mathbf{k} = 0$ . For the fcc structure, the set of seven equations for three unknown variables  $c_{ij}$  has to be solved:  $\rho v_{\alpha,L}^2 = c_{11}$ ;  $\rho v_{\alpha,T}^2 = c_{44}$ ;  $\rho v_{\beta,L}^2 = c_{11} + 4c_{44} + 2c_{12}$ ;  $\rho v_{\beta,T}^2 = c_{11} + c_{44} - c_{12}$ ;  $\rho v_{\gamma,L}^2 = c_{11} + 2c_{44} + c_{12}$ ;  $\rho v_{\gamma,T_h}^2 = c_{11} - c_{12}$ ;  $\rho v_{\gamma,T_3}^2 = c_{44}$ , where the velocities  $v_i$  are the slopes of appropriate acoustic branches. Here,  $\alpha, \beta$  and  $\gamma$  indexes describe three main directions in the reciprocal space  $\langle 0, 0, 1 \rangle$ ,  $\langle 1, 1, 1 \rangle$  and  $\langle 0, 1, 1 \rangle$ , respectively. The density of TiC  $\rho = 4849.6 \text{ kg/m}^3$  was found using the calculated lattice constant. The solution of this set of equations, by means of the least-squares fit, results in  $c_{11} = 5.7$ ,  $c_{12} = 2.5$  and  $c_{44} = 1.51 \text{ MBar}$ . Comparing these values with experimental data (Table 2) one notices considerable discrepancies, especially for  $c_{12}$ . Closer look to dispersion curves, Fig. 2, assures us that the transverse acoustic mode in  $\langle 1, 1, 0 \rangle$  direction and the longitudinal in  $\langle 1, 1, 1 \rangle$  direction do not follow exactly the experimental points. We have checked, that such discrepancy of slope is sufficient to produce the observed deviations of the calculated elastic constants, specially of  $c_{12}$ . The discrepancy in slopes is so small that it could be assigned to the missing force constants describing mainly the long range Coulomb interaction. Indeed, the direct method did not handle well

interactions exceeding the size of the supercell, except for the special points  $\Gamma$ , X, L, W mentioned earlier.

Result	$B$	$c_{11}$	$c_{12}$	$c_{44}$
Exp. $\text{TiC}_{0.91}$ [3]	(2.422)	5.145	1.060	1.788
Exp. TiC [27]	2.4	5.00	1.13	1.75
Exp. $\text{TiC}_{0.95}$ [2]	(2.5)	5.4	1.1	1.8
Exp. $\text{TiC}_{0.89}$ [2]	(2.5)	5.2	1.1	1.8
Calculations [8]	2.2	4.7	0.97	1.67
Ours, acoustic modes	(3.57)	5.7	2.5	1.51
Ours, deform. energy	2.42	5.39	0.94	1.92
Ours, stress-strain	(2.46)	5.21	1.09	1.93

**Table 2.** Experimental and calculated bulk modulus  $B$  and elastic constants  $c_{ij}$  of the TiC crystal, in units of  $10^{11} \text{Nm}^{-2} = 1\text{MBar}$ . Values in parenthesis are calculated from  $B = \frac{1}{3}(c_{11} + 2c_{12})$ .

To rule out that the discrepancy for  $c_{12}$  does not follow from ab-initio calculations, we have derived the bulk modulus and the elastic constants by two conventional methods [8]. The bulk modulus was calculated in the  $1 \times 1 \times 1$  supercell from the total energy as a function of the lattice constant. This data have been fitted to a third order polynomial. Hence, the derivative  $\frac{\partial E}{\partial V}$ , and the bulk modulus  $B$  were calculated from the relation:  $B = -V \frac{\partial E}{\partial V}$ , where  $V$  is the volume of TiC crystallographic unit cell. The  $B$  values are given in Table 2 and they agree quite well with experimental data.

A calculation of  $c_{11}$ ,  $c_{12}$ ,  $c_{44}$  elastic constants involved a similar procedure, in which the crystal was deformed by lengthening and shear deformations. Deformations from 0.5% to 3% in length and from 1 to 5 degrees in angle have been used. The results of small and large deformations are consistent. The deformed lattices have space groups  $\text{Fm}\bar{3}\text{m}$ ,  $\text{I4}/\text{mmm}$  and  $\text{I}/\text{mmm}$ , for bulk expansion, elongation along  $z$ , and sheer modes. In all these deformed lattices all atoms remain in the high-symmetry sites which guaranties an extremum of potential energy at those positions. Thus, in the case of cubic TiC, one is entitled not to carry on the relaxation of internal degrees of freedom during supercell deformations. The calculated elastic constants are compared to experimental data in Table 2. They agree with calculated values given in Ref.[8] and are in good agreement with experiment.

We have also checked the above results using stresses calculated by CASTEP. The elastic constants were found as first derivatives of the stress-strain relationship. For that, we have used the same runs of electronic calculations as for the elastic constant derivation given above using deformation dependence of energy. The results are included in Table 2 and they show slightly better agreement with the experimental data.

In summary, we have shown that the *ab initio* calculations of HF forces, together with the direct method lead to satisfactory description of phonons in the TiC crystal. As usual the frequency of the calculated dispersion curves are slightly too high. The acoustic modes are not sufficiently accurate, thus the elastic constants calculated

from them differ from those found through the supercell deformations. The acoustic part of density of states fits well to neutron experimental data.

The computational advices of J. Oleszkiewicz and the use of facilities of the Computer and Network Center of the Jagellonian University, Cracow, where the calculations have been done, are kindly acknowledged. This work was partially supported by the Polish State Committee of Scientific Research (KBN), grant No 2 PO3B 145 10.

## References

1. L.E. Toth, *Transition Metal Carbides and Nitrides* (Academic Press, New York 1971).
2. L. Pintschovius, W. Reichardt and B. Scheerer, J. Phys. C: Solid State Phys. **11**, 1557 (1978).
3. R. Chang and L. J. Graham, J. Appl. Phys. **37**, 3778 (1966).
4. A. Neckel, R. Eibler, P. Weinberger and K. Schwartz, J. Phys C **9**, 579 (1976).
5. V.P. Zhukov, V.A. Gubanov, O. Jepsen, N.E. Christensen and O.K. Andersen, J. Phys. Chem. Solids **49**, 841 (1988).
6. D.L. Price and B.R. Cooper, Phys. Rev. B **39**, 4945 (1989).
7. J. Häglund, A.F. Guillerment, G. Grimvall and M. Körling, Phys. Rev. B **48**, 11685 (1993).
8. R. Ahuja, O. Eriksson, J. M. Wills, B. Johansson, Phys. Rev. B **53**, 3073 (1996).
9. W. Frank, C. Elsässer, and M. Fähnle, Phys. Rev. Lett. **74**, 1791 (1995).
10. G. Kresse, J. Furthmüller, and J. Hafner, Europhys. Lett. **32**, 729 (1995).
11. K. Parlinski, Z. Q. Li and Y. Kawazoe, Phys. Rev. Lett. **78**, 4063 (1997).
12. G. J. Ackland, M. C. Warren and S. J. Clark, J. Phys.: Condens. Matter **9**, 7861–7872 (1997).
13. M.H.F. Sluiter, M. Weinert, Y. Kawazoe, Europhys. Lett. **43**, 183 (1998).
14. J.S. Lin, A. Qteish, M.C. Payne and V. Heine, Phys. Rev. B **47**, 4174 (1993).
15. J. Goniakowski, J.M. Holender, L.N. Kantorovich, M.J. Gillan and J.A. White, Phys. Rev. B **53**, 953 (1996).
16. M.C. Payne, M.P. Teter, D.C. Allan, T.A. Arias, J.D. Joannopoulos, Rev. of Mod. Phys. **64**, 1045 (1992).
17. CASTEP is a part of *Cerius*<sup>2</sup> system developed by Molecular Simulations.
18. J.P. Perdew, J.A. Chevary, S.H. Vosko, K.A. Jackson, M.R. Pederson, D.J. Singh, C. Fiolhais, Phys. Rev. B **46**, 6671 (1992).
19. J. Goniakowski, J. M. Holender, L. N. Kantorovich, M. J. Gillan, J. A. White, Phys. Rev. B **53**, 957 (1996).
20. H.J. Monkhorst and J.D. Pack, Phys. Rev. B **13**, 5188 (1976).
21. I. Náray-Szabó, *Inorganic Crystal Chemistry* (Akadémiai kiadó, Budapest, 1969), p.301.
22. A. García, C. Elsässer, J. Zhu, S.G. Louie, M.L. Cohen, Phys. Rev. B **46**, 9829 (1992).
23. Y.M. Juan and E. Kaxiras, Phys. Rev. B **48**, 14 994 (1993).
24. K. Seifert, J. Hafner, J. Furthmüller, G. Kresse, J. Phys. Condens. Matter **7**, 3683 (1995).
25. W. H. Press, B.P. Flannery, S.A. Teukolsky, and W.T. Vetterling, *Numerical Recipes* (Cambridge Univ. Press, 1988), p.301.
26. F. Gompf and W. Reichardt, 1977, unpublished.
27. M. M. Choy *et. al.*, *Numerical Data and Functional Relationships in Science and Technology* (Springer, Berlin, 1979), vol.11.